



# Geomorphic response of bedrock landslides induced landscape evolution across the Teesta catchment, Eastern Himalaya

Abhishek Kashyap<sup>1</sup> · Mukunda Dev Behera<sup>1</sup>

Received: 21 November 2022 / Accepted: 9 March 2023 / Published online: 6 April 2023  
© The Author(s), under exclusive licence to Springer-Verlag GmbH Germany, part of Springer Nature 2023

## Abstract

Bedrock landslides are the primary agent of hillslope erosion, and mass wasting, and an essential source of sediment flux to the fluvial network in the mountainous terrain, in particular, in the Himalayan mountain belt. To understand the characteristics of the landscape, we calculate geomorphic matrices including the topographic variables, longitudinal and topographic swath profile, channel steepness index, and stream length gradient index to analyze the spatial distribution of landslide occurrences over landscape evolution. The intensity of rainfall gradient and topographic variables were spatially correlated with the erosion and exhumation rates of the studied catchment. Our analysis suggests that the zones with slope ranges of 24°–28°, relief ranges of 800–1000 m, and elevation ranges of 1500–1700 m, which coincide with the rainfall intensity range of 2500–2700 mm/year in the Teesta river catchment, have the highest probability of frequently occurring landslides. Higher tectonic activity is principally responsible for the landslide over the Higher Himalaya to the north of the Main Central Thrust (MCT)–Main Boundary Thrust (MBT) along the orographic barrier. In contrast, litho-tectonics regulates and mostly triggers landslides adjacent to the MCT–MBT structural affinity dominated by rainfall intensity. Our observation suggests that erosion rates frequently exceed long-term exhumation rates and are spatially more variable. Moreover, they exhibit significantly divergent spatial patterns, which suggests that the processes governing these rates are independent. Exhumation rates have been shown to decrease from south to north over geological periods, rising in the southwest region at ~1.2 mm/year and decreasing to ~0.5 mm/year in the northernmost region of the Teesta catchment. Long-term exhumation rates are not correlated with geomorphic or climatic variables. The highest apparent erosion rates (5 mm/year) are seen in the catchment that crosses the MCT Zone, however, these rates appear to have been severely impacted by recent landslides. Conversely, changes in rainfall rate do not appear to significantly impact either rate of long-term exhumation or erosion in the Teesta catchment.

**Keywords** Landslides distribution · Rainfall gradient · Topographic variables · Landscape evolution

## Introduction

Landslides are a common occurrence in the tectonically active mountains and have an effect on how the landscape evolves (Korup et al. 2007, 2010). According to many authors (Koons 1989; Montgomery et al. 2001; Korup et al. 2010), the topographic development of mountain belts can be viewed as a competition between tectonic fluxes of

material into the orogen, modulated by geodynamic processes such as crustal faulting or lithospheric deformation, and erosional fluxes of material out of the orogen, modulated by Earth surface processes (Korup et al. 2007). In an active mountain belt changes in local relief have even less effect on regulating landscape-scale erosion rates, while erosion rates adjust to high rates of tectonically driven rock uplift primarily through changes in the frequency of landsliding rather than hillslope steepness (Montgomery and Brandon 2002). Landslides, which contribute to mountain erosion by moving debris from slopes to valley bottoms, are frequently influenced by tectonics, climate, and anthropogenic activities (Kumar et al. 2021; Gupta et al. 2022). On a local level, landslides are acknowledged as being significant agents of mass wasting and hillslope evolution; however, it is unclear how much of an overall influence they play in

✉ Mukunda Dev Behera  
mdbehera@coral.iitkgp.ac.in

Abhishek Kashyap  
kashyap95abhishek@kgpian.iitkgp.ac.in

<sup>1</sup> Centre for Oceans, Rivers, Atmosphere and Land Sciences (CORAL), Indian Institute of Technology Kharagpur, Kharagpur, West Bengal 721302, India

the development of mountainous topography (Korup et al. 2010).

In the Himalaya, lithology, structural characteristics and rainfall intensity have a significant impact in the development of landslides (Jamir et al. 2020). According to Gupta et al. (2017), the main natural factors are an increase in extreme rainfall events and concentrated flash flooding, especially during the monsoon season. The frequency and size of landslides, as well as the events connected with mass movement, have, however, multiplied in recent years across the Himalayan terrain (Gupta et al. 2022). Approximately 15% of India's landmass is vulnerable to various landslides, which are primarily located in the Himalayan region (BMTPC 2003). For the country as a whole, a reasonable estimate of the financial loss is in the range of \$20 million USD each year at 2011 pricing, which is about 30% of the overall damage caused by landslides worldwide (MHA, Govt. of India, 2011). It is important to note that landslides in the Himalaya do not occur randomly but rather only in specific areas designated as hotspots for landslides (Gupta et al. 2022). Landslides generated by bedrock transport significant amounts of sediment and impact landscape. However, the interactions between fluvial systems and debris produced by landslide, which collectively control the evolution of large-scale landscapes, are not well understood (Campforts et al. 2022). The Teesta catchment in the eastern Himalaya is known for its frequent and catastrophic landslides (Anbarasu et al. 2010; Bhasin et al. 2002). Despite the fact they are frequently driven on by earthquakes or even the monsoon season (Bhasin et al. 2020; Singh and Singh 2016; Weidinger and Korup 2009), their spatial distribution suggests that local factors are all in responsible for their occurrence. These regions also lie in the seismic Zone IV, the second-highest seismic zone on the Seismic Zonation Map of India (BIS code 2002), suggesting high vulnerability to hazard. The present study aims to characterize the spatial landslides occurrence over the topography and climatic variables and understanding their role in landscape evolution process across the Teesta catchment in eastern Himalayas.

### Regional seismo-tectonic setting

There are numerous significant north-dipping faults that divide different geological domains in the Himalayan mountain region (Hodges 2000; Yin 2006). The South Tibetan Detachment (STD), Main Central Thrust (MCT), Main Boundary Thrust (MBT), and Main Frontal Thrust (MFT) are these (BIS code 2002), in that order having decreasing initiation ages from north to south (Yin 2006). The Tethyan Sedimentary Sequence (TSS), a sedimentary succession from the Palaeozoic to the Eocene that was deposited on the Indian passive margin, is found in the northernmost region (Liu and Einsele 1994). The Greater Himalayan Sequence

(GHS) and the TSS are separated by the extensional STD, which was active in the Early-Middle Miocene (Burchfiel et al. 1992; Kellett et al. 2013). In Sikkim Himalayas, between two branches of the MCT, lies a heavily sheared zone known as the Main Central Thrust Zone (MCTZ) (Bhattacharyya and Mitra 2009; Kellett et al. 2014). The Lesser Himalayan Sequence (LHS), which is exposed in the Teesta tectonic half-window, is made up of greenschist-facies meta sedimentary rocks and is found in the footwall of the MCTZ (Abrahami et al. 2016). High-grade metamorphic rocks from the GHS and MCTZ emerge south of the Teesta half-window and are exposed up to a few kilometres from the mountain front in the Darjeeling klippe (Mitra et al. 2010). The Main Boundary Thrust (MBT), which is made up of distorted Mio-Pliocene foreland catchment sediments from the Siwalik Group, forms the southern boundary of the LHS and divides it from the Sub-Himalaya (Mukul 2000). The active Main Frontal Thrust (MFT), which forms the contact between the Siwalik Group and the Quaternary deposits of the Ganga–Brahmaputra plain, is the Himalaya's most exterior thrust. Over the past thousand years, it has hosted several significant surface-breaking earthquakes. The majority of the moderate earthquakes ( $M_w > 4.5$ ) that have been detected in Teesta catchment have had frequent epicentres and have occurred between the MBT and the MCT (Hazarika and Ravi Kumar 2012; Mukul 2010). Based on these findings, Mukul (2010) hypothesises that out-of-sequence deformation in a sub-critical wedge, localised in the Lesser Himalaya, can explain the active tectonics of the Teesta catchment in eastern Himalayas (Fig. 1).

### Regional geomorphic setting

Transects through the Himalaya demonstrate two distinct topographical and rainfall patterns: (i) a more or less linear increase in elevation and relief accompanied by a single peak of rainfall close to the mountain front; or (ii) a significant increase in elevation and relief around the MCTZ, accompanied by a double peak of rainfall, one at the mountain front and the other at the locus of the steep topographic gradient (Bookhagen and Burbank 2006, 2010). The Teesta catchment acts as a nexus between the central and eastern Himalayan landscape. As a result, a single peak of rainfall along the eastern mountain front divides into two bands further west. Two bands of rainfall, each exceeding  $\sim 5$  (m/year) along the southern edge of the LHS and  $\sim 6$ – $7$  (m/year) coincident with the MCTZ north of the Teesta half window, are plainly visible on a transect across the Teesta catchment (Bookhagen and Burbank 2006, 2010; Abrahami et al. 2016) (Fig. 1). Teesta is one of the Himalayan bedrock river having a significantly convex shape and three significant knick-zones (Brookfield 1998). Near the boundary between Sikkim and Tibet, at an elevation of 5320 m, Lamo Cho serves as the source of the Teesta river. Before bending

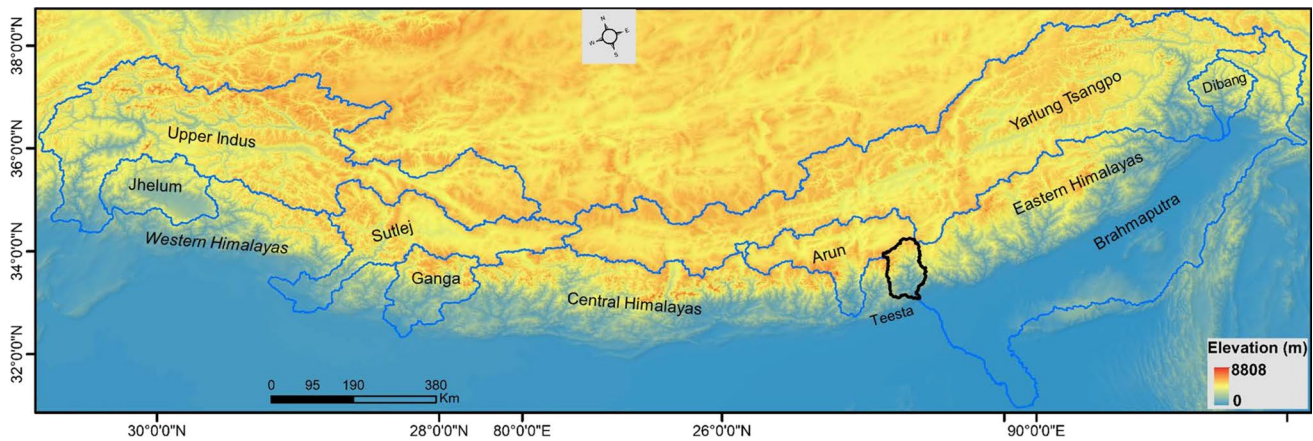


**Fig. 1** The topography of the Himalaya–Tibet system overlaid with the Teesta river catchment (black) along with major river catchments boundaries (location map)

south and crossing through the Sikkim Himalaya, the Teesta river travels westward with a fairly low gradient for about 20 km. Only 150 m above sea level, 200 km downstream, the river traverses the Himalayan mountain range before joining the Brahmaputra in Bangladesh. It has created a fluvial megafan in the foreland known as the Teesta megafan throughout the Quaternary (Chakraborty and Ghosh 2010). The Teesta river catchment has an asymmetrical drainage pattern, with many short tributaries to the east and many longer ones with bigger drainage catchments that considerably contribute to the flow of the main Teesta river. Around the Kanchenjunga massif, western tributaries drain severely glaciated terrain with significant snowfields (8586 m). As opposed to the western tributaries, the eastern tributaries come from considerably smaller, semi-permanent snowfields. The 8000 km<sup>2</sup> catchment is made up of around 250 km<sup>2</sup> of permanent snowfields and glaciers, and seasonal melting greatly affects the Teesta River's average annual discharge (Krishna 2005). The Teesta catchment across the eastern Himalayan landscape frequently experiences landslides (Basu and De 2003). Both pre disposing elements, such as geology, slope, or glacial debuttressing, and either rainfall or seismic triggering can be implicated in these mass-movement occurrences. With the exception of road construction in north Sikkim, human development appears to have increased the frequency of landslides (Mehrotra et al. 1996). In the field, we discovered that the MCTZ and the steep gorges in the northernmost catchments are where landslides are most frequently found.

## Materials used and methodology

In order to minimise null-error, we resampled the data using ArcGIS's "elevation void fill function" after processing open source satellite-derived Shuttle Radar Topographic Mission

(SRTM)-30 m; (<http://srtm.csi.cgiar.org/>) spatial resolution topography datasets for landscape characterisation (Lehner et al. 2008). We extracted the drainage network and drainage divide of the Teesta river systems in the Sikkim Himalaya using the D8-algorithm (O'Callaghan and Mark 1984), taking MFT as a base level. To understand its role in the process of regional erosion, rainfall data for the past 21 years (2001–2021) has been obtained from (NASA–LP DAAC open source site) monthly datasets with 0.1° spatial Resolution from the Global Precipitation Measurement (GPM). Landslide inventory spatial datasets are obtained from Geological Survey of India's Bhukosh portal (<http://bhukosh.gsi.gov.in/>), whereas earthquake spatial datasets can be taken from the NASA-USGS open source platform (<https://earthquake.usgs.gov>). From previously published literatures, the geology, tectonic characteristics, and geographic location of denudation rates and exhumation rates of the Teesta river catchment are compiled (SM1; Abrahami et al. 2016) (Table 1).

In the present study, we used elevation data to calculate topographic attributes such as slope and relief and spatial analysis of seasonal and annual mean rainfall using ArcGIS. Due to the regional context of the present study, the relief map is produced by passing a 900 m rectangle radius focal range window, and the slope map is produced by passing a 500 m radius mean filter over the slope model from the DEM (Jaiswara et al. 2019a, b). Using the "extract multi values to a point" function in ArcGIS, the geographic distribution of landslide points over topography variables such as elevation, slope, and relief as well as climatic attributes such as rainfall gradient are extracted. In order to determine the highest probability density frequency for the spatial landslides occurrences over the topographic and climatic variables in the studied bedrock river catchment, the extracted gridded value datasets are further analysed through statistical

**Table 1** Materials used and data source

Data used	Name	Type	Resolution	Source
Topography	SRTM	Raster	30 m	SRTM-CGIAR
Precipitation	GPM	Raster	0.1°	NASA-LPDAAC
Landslides Inventory	Landslides points	Vector	–	GSI-Bhukosh
Geology	Lithology structure	Vector	–	GSI-Bhukosh
Earthquake location	Earthquake distribution	Vector	–	NASA-USGS hazard portal

analysis. Transient-Profiler and TopoToolbox are used in the MATLAB platforms for the quantitative landscape modelling using geomorphic indices from Digital Elevation Models (Jaiswara et al. 2019a, 2020; Schwanghart and Scherler 2014). For the landscape characterization, the Teesta catchment is divided into five sub-catchments, namely S1–S2–S3–S4–S5. Using the following proxies, we evaluate the spatial interrelationship of the regional landscape with the factors that influence the occurrence of landslides in the Teesta river catchment (Fig. 2) (Bull 2008).

**Topographic distribution: hypsometric integral (Hi) (Keller and Pinter 1996), slope frequency and swath profile**

The hypsometric integral (Hi) in a drainage catchment represents the relative distribution of elevation in a given section of the landscape (Strahler 1952). Since the Hi describes the percentage of the region below the hypsometric curve that indicates the volume of a catchment that has not been eroded, it serves as a stand-in for the catchment’s maturity

stage (Strahler 1952). For the studied catchment, we derive slope frequency and hypsometry curves to describe the spatial heterogeneity in the erosional response with regard to the base level. The spatial variability of the landscape is defined by these fundamental parameters, which also aid in determining the variance in the regulating elements (Strahler 1952; Schumm 1979).

$$H_i = (h_{mean} - h_{min}) / (h_{max} + h_{min}) \tag{1}$$

where Hi is the hypsometric integral and hmax, hmin, and hmean are, respectively, the highest, the minimum, and the mean elevation. Therefore, a high hypsometric integral denotes a young or youthful stage of a landscape, whereas intermediate to lower values suggest an older or mature stage as the landscape is being eroded (Strahler 1952).

We used swath profiles, which combine spatial elevation data into a single profile, to evaluate regional landscape variation with tectonic and erosional features (Andreani et al. 2014). As opposed to conventional profiles, where topography is taken from a single line, this method uses

**Input Parameters**

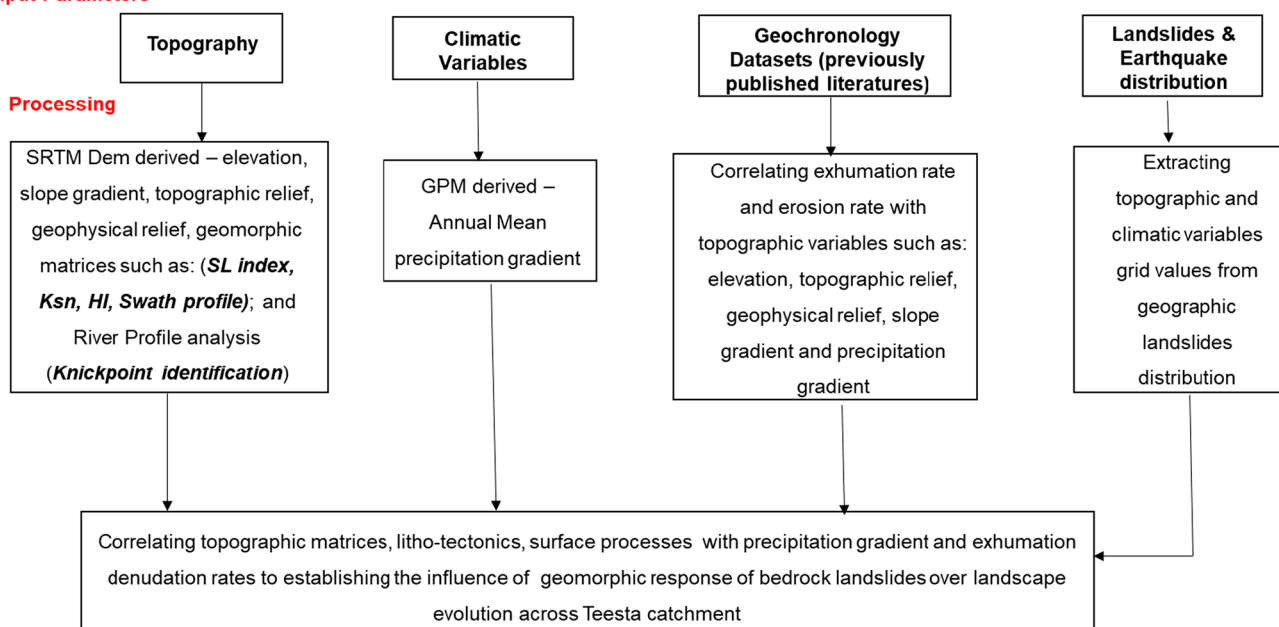


**Fig. 2** Methodological flow chart

a rectangular swath. Then, statistical parameters (often the maximum, minimum, and mean elevations) are determined using elevation data projected onto a vertical plane parallel to the long axis of the swath rectangle. The valley floors are represented by the minimum elevation curve. Calculating the arithmetic difference between the maximum and minimum elevations provides a rapid estimation of the incision.

### Geophysical relief: minimum eroded rock column

The geophysical relief of a region calculates the minimum cumulative eroded column in a landscape under the assumption of a hypothetical pre-incision surface, which is obtained by extrapolating the elevation from the current drainage divides to the corresponding riverbed under the presumption that erosional processes have no impact on drainage divides (Abbott et al. 1997; Small and Anderson 1998; Brocklehurst and Whipple 2002). To comprehend long-term erosion localisation throughout the examined river catchment, the spatial variability of the geophysical relief has been correlated with the Normalized steepness index (Ksn) and previously documented denudation rates.

### River profile analysis

#### Stream-length gradient index (SL-profile)

A sensitive indicator for analysing the reach scale variability of tectonic function, rock resistance, and topography is the stream length-gradient index. Rivers that flow across different types of material, such as rocks and soils, tend to reach equilibrium with particular longitudinal profiles and hydraulic geometries (Hack 1973; Bull 2007). In a river catchment, it can be used to determine the relative tectonic activity (Keller and Pinter 2002; Whittaker et al. 2007).

SL index has calculated using the formula followed by Keller and Pinter (2002):

$$SL = (\Delta H / \Delta L) / L \quad (2)$$

where,  $L$  is the total river length from the midpoint of the chosen reach whose index is calculated, to the highest point on the channel,  $\Delta H / \Delta L$  is channel slope or gradient of the reach in which  $\Delta H$  is a change in elevation for a particular channel of the reach with respect to  $\Delta L$  which represents the length of the reach.

#### Knickpoint identification

The continuous breaks in the linear pattern in the log scaling relationship between drainage area and slope gradient is defined as the slope-break knickpoints (Kirby and

Whipple 2012). It indicates the continuity break in the longitudinal river profile, where the upstream segment represents the Uplift–Erosion (U–E) of the current transient regime, while the downstream portion represents the previous U–E setting (Whipple et al. 2013). These knickpoints formed due to the change in the base level and driving the fluvial system from one steady state to another (Wobus et al. 2006).

#### Steepness index: slope-area analysis

The shape of the river profile largely determines the topographic relief of the erosional landscape. A normalised steepness index (Ksn), which allows for a fair comparison across the catchments despite their drastically varied areas, was calculated using the reference concavity (ref) (Wobus et al. 2006). The power law relationship between the local channel slope ( $S$ ) along the river profile segment and the related contributing drainage area ( $A$ ) may be used to depict the steady-state graded profile that rivers often have (Flint 1974):

$$S = ksA^{-\theta} \quad (3)$$

where  $ks = [U/K]^{1/n}$  is the channel steepness index,  $\theta = m/n$  is the channel concavity index,  $m$  and  $n$  are positive constants,  $U$  is the rock uplift rate [erosion rate ( $E$ ) at a steady state], and  $K$  represents the bedrock strength and/or climate. According to Wobus et al. (2006) and Kirby and Whipple (2012), a normalised steepness index (Ksn) was calculated at the reference concavity ( $\theta_{ref}$ ) 0.45, allowing a fair comparison across all sub-catchments despite their significantly different areas. This  $\theta_{ref}$  was used to calculate the regional Ksn of the river catchment.

### Results

Among the Himalayan river systems, the Teesta is unique as a fully developed  $\sim > 400$  km long seventh-order drainage originates from a glacial lake at  $\sim 6000$  m in the Tibetan plateau enters the Himalayan terrain as antecedent channel cutting across the seismically active mountain belt without any lateral deviation. In the Himalayan terrain, the river passes through three major fault systems namely, the MCT, MBT, and MFT, forms multiple loops parallel and transverse to the regional structural trend before debouching to the Brahmaputra plains at  $\sim 50$  m elevation, which affected the Himalayan tectonics and topography. The Teesta catchment receives focused rainfall along the neotectonically active Sub Himalayan mountain front, thereby making it an

ideal case for exploring the spatially varying interaction of rainfall-driven erosion processes with the setting (Fig. 3).

### Landslides distribution over landscape characterization

Due to its higher relief variation, slope gradient, and topographic ruggedness, the Teesta catchment experiences more landslides compared to any other catchment in the eastern Himalayas. The spatial distribution of bedrock landslides in the studied catchment shows the spatial heterogeneity

of tectonics and climate linkage in regulating surface processes. To understand its significance in the landscape evolution, we examined the distribution of landslides as a function of the erosion process at the catchment scale. The characteristics of spatial distribution indicate that the areas with the highest probability density frequency of landslides occurring are those that have slopes range  $\sim 24^\circ\text{--}28^\circ$ , relief range  $\sim 800\text{--}1000$  m, and elevation range  $\sim 1500\text{--}1700$  m, which tends to fall within the  $\sim 2500\text{--}2700$  mm/year range of rainfall erosivity region (Fig. 4).

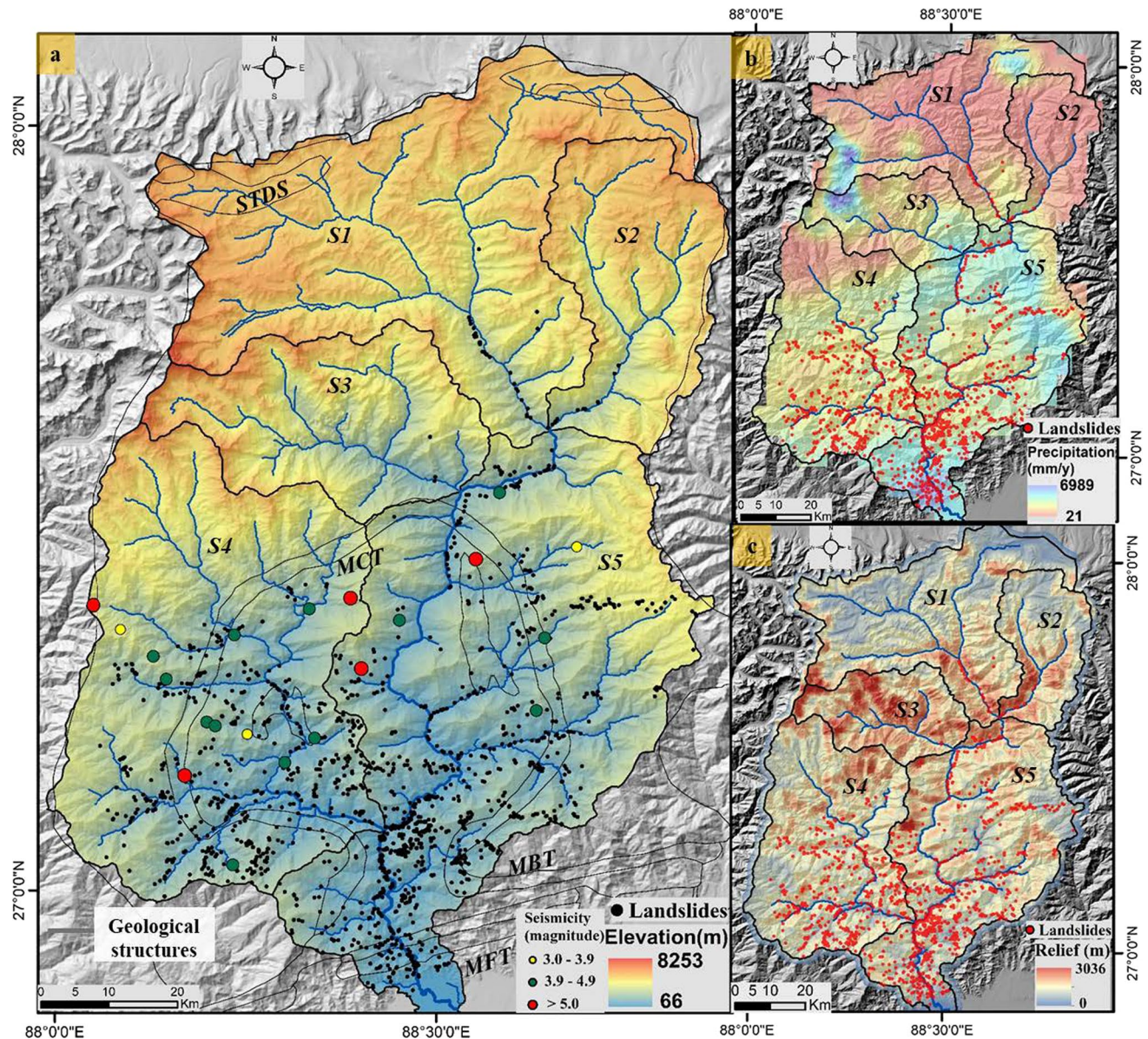


**Fig. 3** a Regional topographic and seismotectonic setting of Teesta catchment overlaid with major geological structures (*MFT* main frontal thrust, *MBT* main boundary thrust, *MCT* main central thrust, *STDS* Southern Tibet Detachment system), sub-catchments (S1, S2,

S3, S4, S5), earthquake and landslides distribution. **b** Spatial distribution of annual mean precipitation pattern along the studied area overlaid with landslides distribution. **c** Spatial distribution of topographic relief overlaid with landslides distribution across the studied area

We generated the hypsometric integral (Hi) using hypsometric curves and plotted the slope frequency distribution of the studied river sub catchments in order to understand the role of landslides distribution in the landscape evolution. With higher Hi values of 0.49 and 0.57, respectively, the elevated terrain of the Teesta River sub catchments S1 and S2 exhibits a youthful landscape. A mature landscape can be seen in the sub catchments S3, S4, and S5, which have lower Hi values of 0.41, 0.30, and 0.33, respectively (Fig. 5b). The higher Hi values indicate a greater incision and regeneration of the terrain, which is also evident in the relief and slope pattern. This suggests that erosional interaction with active tectonics varies spatially, providing the distinctive spatial variability in the landscape. In order to analyse the landscape association with the occurrence of landslides in the Teesta river catchments, we exhibited the slope distribution pattern of the analysed river catchments, which follows a power-law with a bell-shaped slope frequency distribution. The sub-catchments S3, S4, and S5 in the high relief zone exhibit a Gaussian distribution with a mean slope of roughly  $25^{\circ}$ – $30^{\circ}$ , indicating greater roughness. The mean slope of the sub catchment S1 and S2 shows Weibull distribution pattern with mean slope ranges  $15^{\circ}$ – $25^{\circ}$  (Fig. 5c).

## Geomorphic impact of landslides process over river profile

The normalised steepness index (Ksn), the slope-break Knickpoint, and the SL-Index profile has been used to analyse the tectonic association and the landscape response in the landslide process along the Teesta river profile. We drive SL-index and Ksn profile for all five extracted sub-catchments of Teesta catchment and analyze the river gradient profile across the landslides occurrence regions. The zone of topographic breaks across the active structures clearly corresponds to the spike or transition of the SL index and Ksn (Kirby et al. 2005). The stream gradient value increases along the transverse length of the channel at lower elevations, while it decreases in segments that run parallel to the structural trend or in the zone of abandoned misfit channel (Figs. 5a, 6a). The terrain along the swath profile indicates that the tectonically active Sub Himalayan front, which is also the region of high annual rainfall permitting high landscape erosion, has experienced very high incision (Fig. 6b). The SL index and Ksn both exhibit the same pattern, which may suggest tectonic-climate coupling. The Lesser Himalayan region channel segment corresponds closely to the structural trend in the region and exhibits progressive expansion of relief with low SL index and Ksn (Fig. 6c, d).

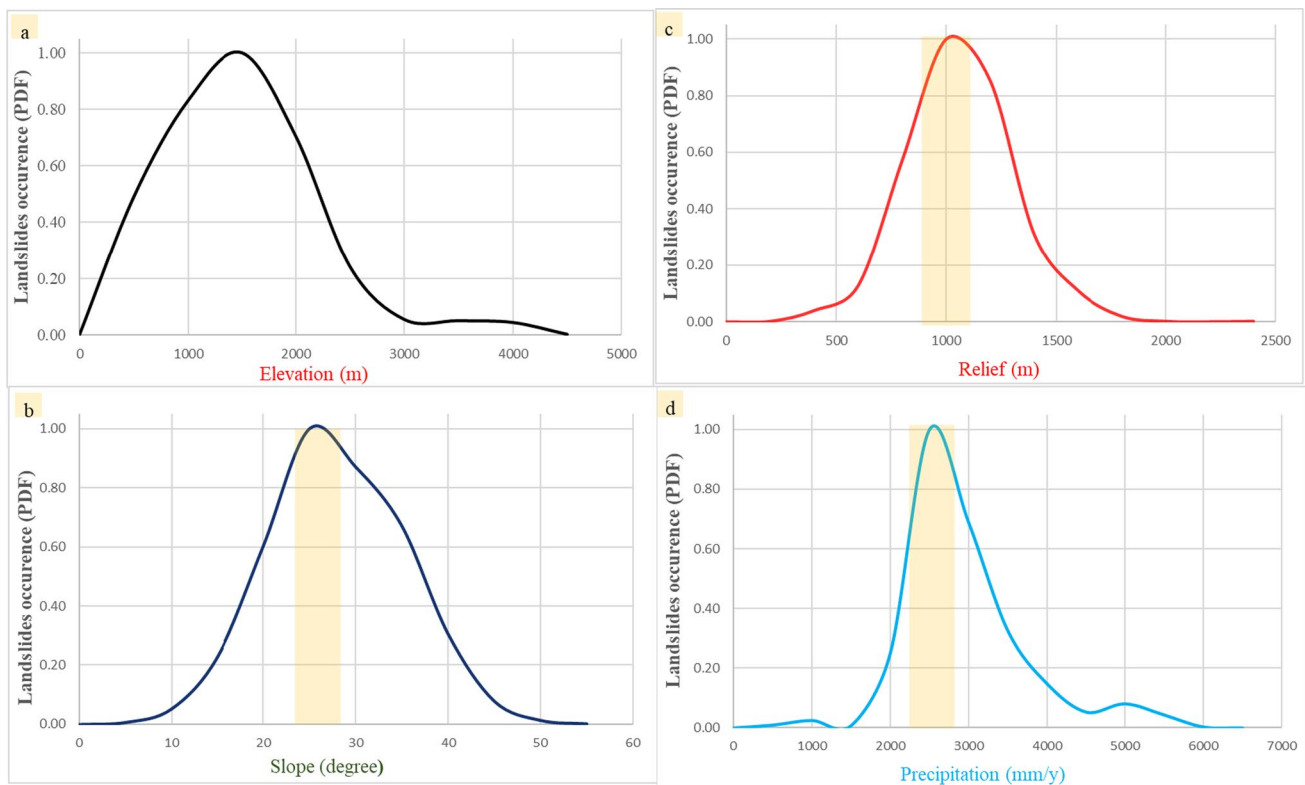


**Fig. 4** The Relative Probability Distribution (PDF) of landslides occurrences across **a** elevation, **b** slope, **c** relief, **d** annual mean precipitation; in the studied river catchment

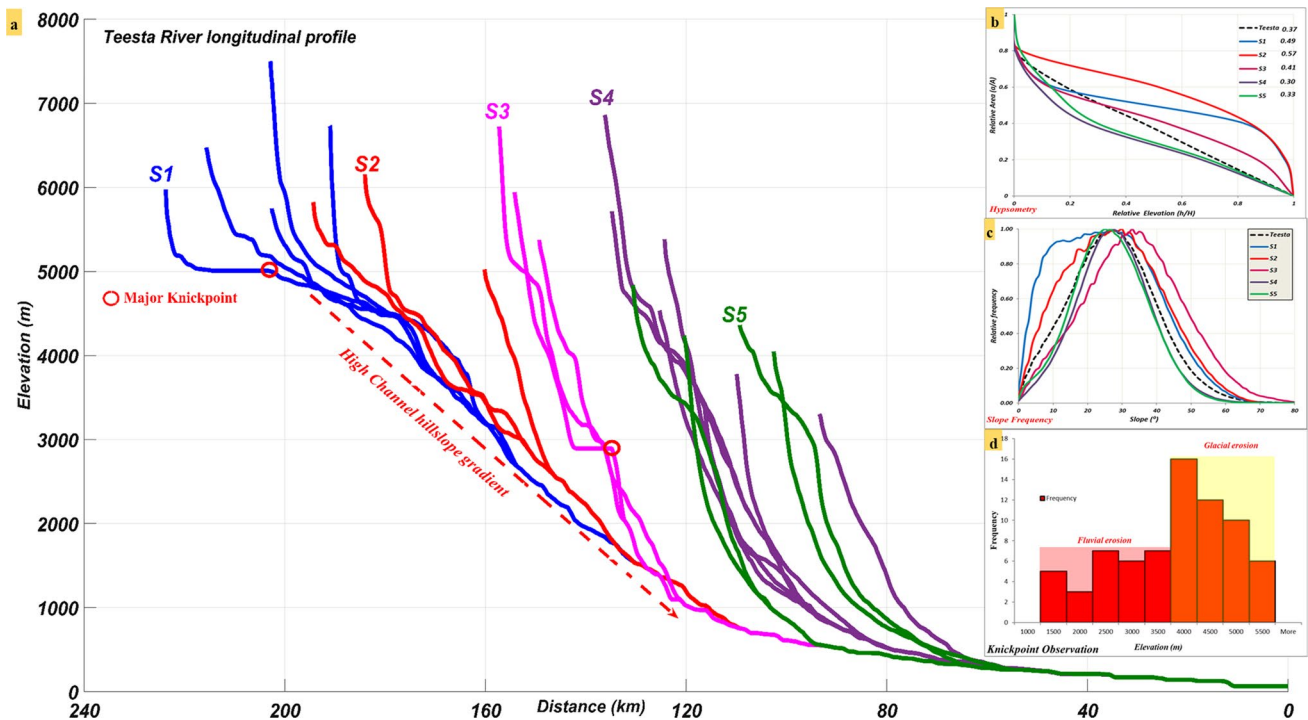


**Fig. 5** **a** Longitudinal river profile of Teesta river along with sub catchment tributaries overlaid with major Knickpoint; **b** hypsometric curve and hypsometric integral of the studied river catchment and

sub catchment; **c** mean slope frequency curve of the studied river catchment and sub catchments; **d** histogram distribution of observed Knickpoint across the studied catchment

Although the slope processes in the glacial-fluvial regime dominate the landscape gradation, these indices are high toward the Higher Himalayan zone in the north. The transition from the upstream relict segments to the actively incising downstream segment is marked by major slope-break knickpoints along the tributaries of the Teesta river at an elevation of 2000–3500 m suggesting fluvial erosion process and 4000–5500 m showing glacial erosion process (Figs. 5d, 7a). The region of high erosion is identified by the knickpoint zone as well as a high Ksn.

It has been observed that the distribution of Knickpoints, the frequency of landslides, and topographic relief are all associated with the spatial variability of the normalised Ksn for the Teesta catchment, which ranges from (0–47)  $m^{0.9}$ . Higher Ksn values were associated with the spatial distribution of landslides, which suggests a higher incision regime in a region 200 km away from the MCT along the downstream. We describe the Ksn values in the quantile distribution, which divide the observation's range into discrete intervals with comparable probabilities. According to the Ksn distribution, downstream channel portion of the Teesta river catchment have higher Ksn values ( $\sim 47 m^{0.9}$ ), which indicates greater dynamic incision, whereas upper channel segments have lower Ksn values, which indicates relative erosional quiescence. Higher relief ranges are proportionally correlated with high Ksn values along the STDS-MCT

structural affinity, according to the Ksn values overlaid over topographic relief. The Ksn range and topographic relief variation suggests that the Teesta catchment has a range of characteristics such as, the first one in the Tethyan-Higher Himalayan sequence across the STDS-MCT, where Ksn achieves its highest values ranges from  $\sim 11$ – $47 m^{0.9}$  and relief ranges at about (2500–3500 m). Seismicity distribution in the litho-tectonic setup in this zone indicates active tectonic interference, which also acts as the primary trigger for the initiation of landslides as a consequence of erosion along the downstream segment. Across MBT–MFT in the downstream segment, the Ksn intensity and relief both decrease toward the lower Himalayan sequence. Landslides occur on the northern side of the higher Himalayas over a litho-tectonic configuration, and the spatial distribution of regional earthquakes there suggests that this is a primary driving force for topographic interaction.

### Landslides mechanism over landscape evolution

The spatial erosion efficiency is demonstrated by the Ksn distribution, and it can be long-term estimated in the form of geophysical relief, which calculates the minimum eroded column taking the drainage divide into equilibrium state. To understand long-term Uplift-erosion localization in the Teesta river catchment, the spatial variability of the



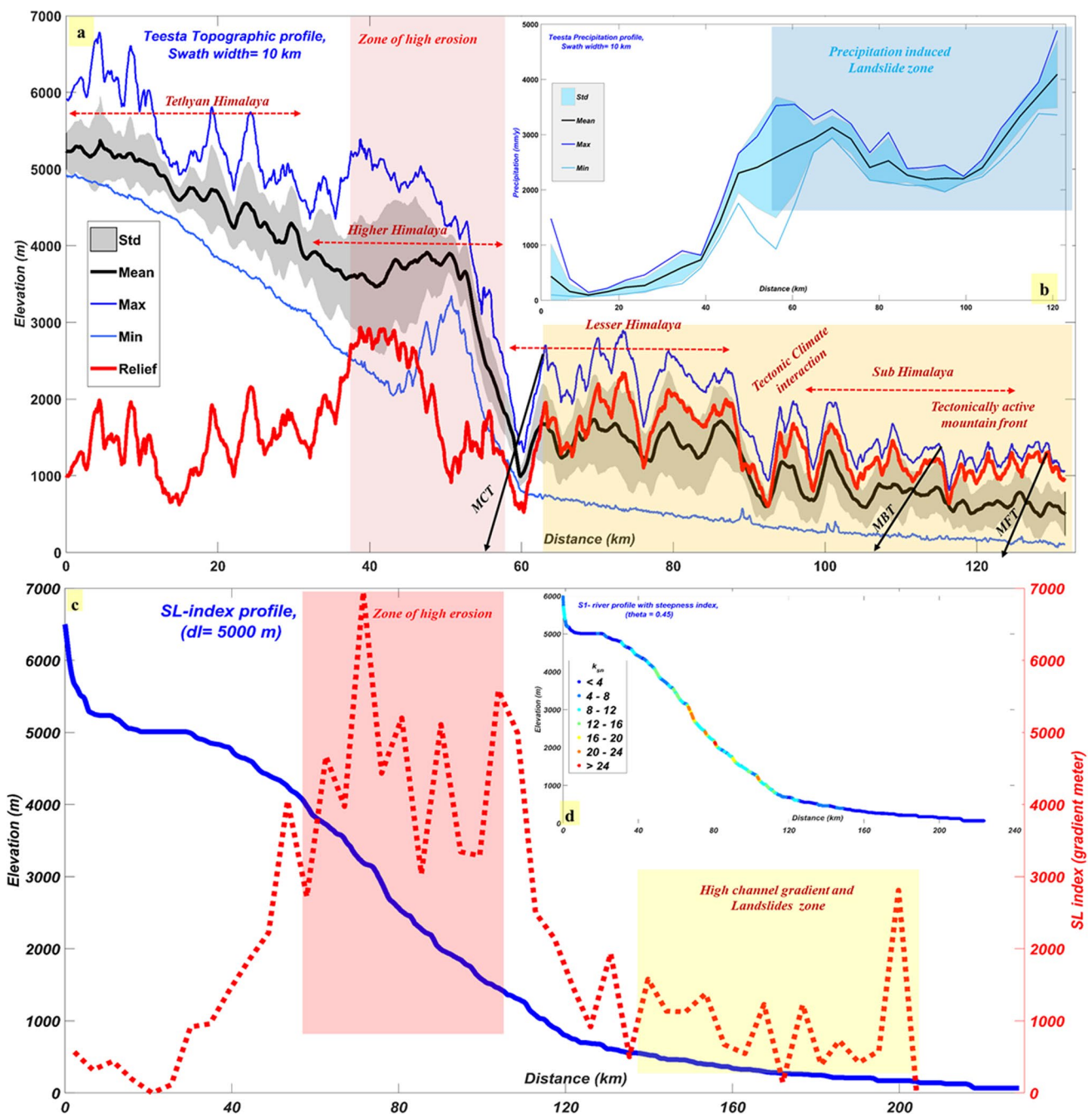


**Fig. 6** a Swath profile of the elevation in the Teesta catchment. b Swath profile of the precipitation data in the Teesta catchment. c The trunk channel profile of Teesta river plotted with SL-index. d The trunk channel profile Teesta river plotted with Ksn

geophysical relief has been coupled with the Ksn, Denudation rates, Exhumation rates, and Landslides datasets. For instance, the STDS and MCT structural affinity show maximum geophysical relief ranging ranges of (3–4) km, second along downstream segment of MCT and MBT

structural affinity ranges of (2–3.5) km, and third along MCT–MBT structural association ranges of 3 km. These three distinct areas across the Teesta river catchment exhibit a characteristics geophysical relief distribution ranges from (0–4) km. Maximum erosion is visible in the sub-catchment

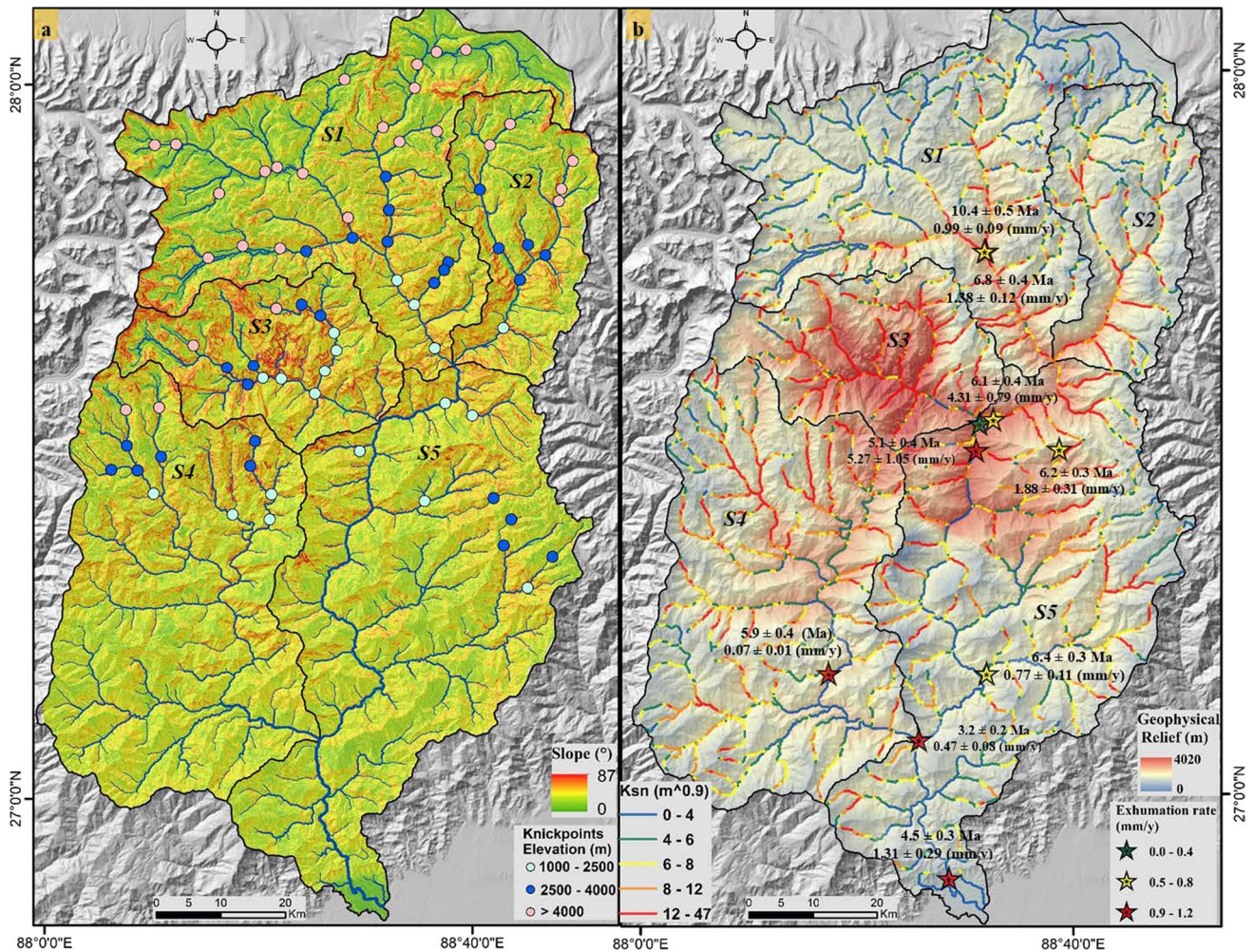


**Fig. 7** **a** Spatial distribution of observed Knickpoint over the slope gradient across studied river catchment; **b** spatial distribution of geophysical relief overlaid with exhumation rates (taken from previously published literatures referred: SM1) of the studied river catchment

S3 adjacent to S4–S5, and it reduces southward to around 0–200 m along the MFT. We analysed the spatial variation as the function of landslides-driven incision to understand coupling of landslides dynamics and long erosion that may have implications on landscape evolution of the region due to the close association of high Ksn-geophysical relief with the active structures across the studied catchments (Fig. 7b).

In order to understand the role of bedrock landslides in the landscape evolution process, we quantified the spatial inter-relationship between previously published geochronology datasets such as denudation rate and exhumation age in the studied river catchment with topographic matrices and rainfall

intensity. The statistical trend analysis shows that the observed erosion rate has a direct linear relationship with slope gradient, geophysical relief, and rainfall intensity but an inverse relationship with topographic matrices. However, the exhumation rate has a linear proportion relationship with topographic variables including elevation, relief, and slope gradient and an inverse relationship with geophysical relief and rainfall intensity (Figs. 8, 9). Our observation signifies that the bedrock landslides may be the primary contributor to erosion and the main source of sediment supply to rivers in the higher to lesser Himalayas on geological timescales.

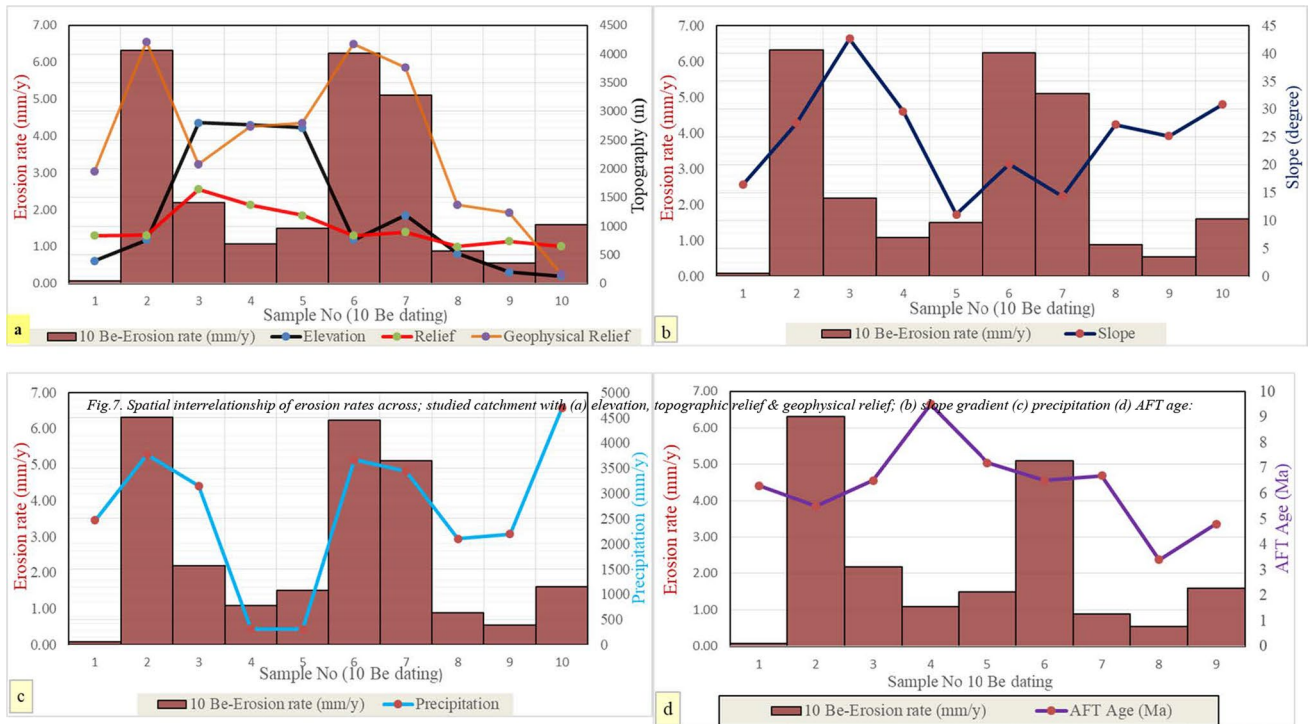


**Fig. 8** Spatial interrelationship of erosion rates across; studied catchment with **a** elevation, topographic relief and geophysical relief; **b** slope gradient, **c** precipitation, **d** AFT age

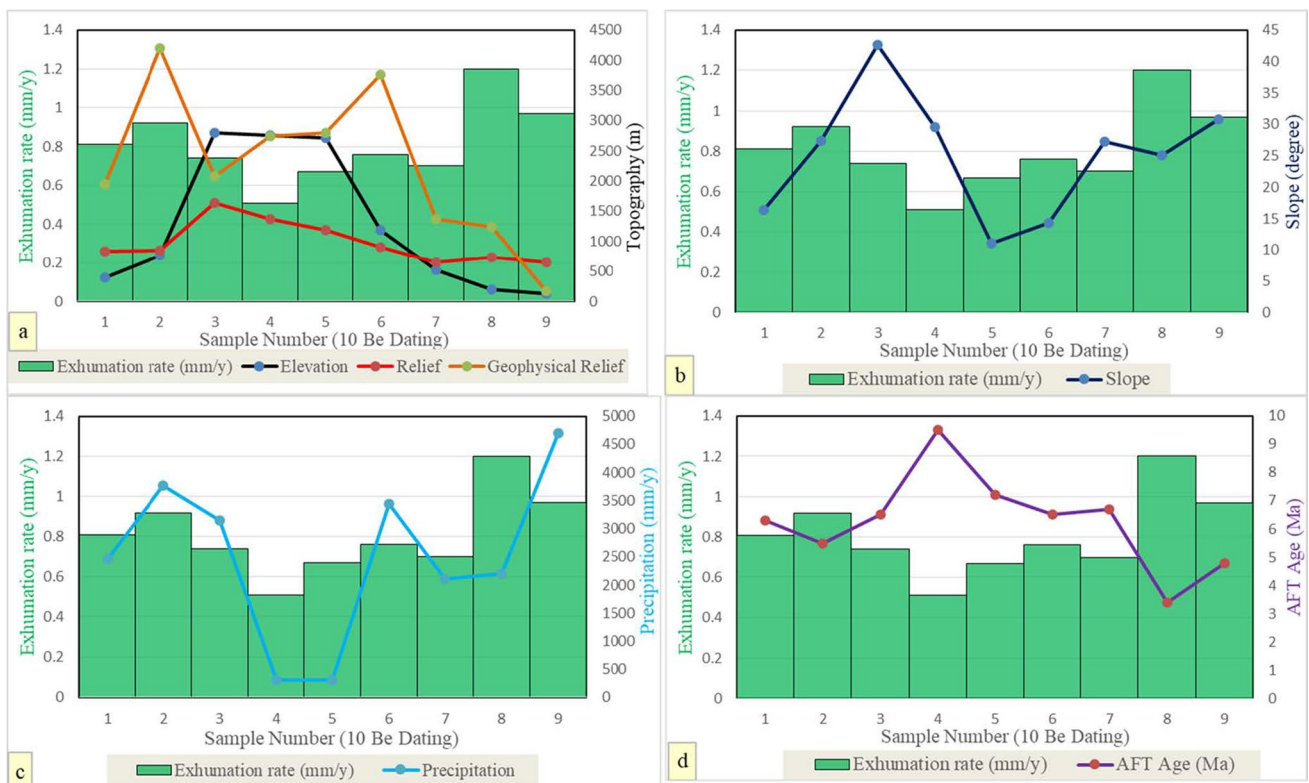


**Fig. 9** Spatial interrelationship of exhumation rates across; studied catchment with **a** elevation, topographic relief and geophysical relief; **b** slope gradient, **c** precipitation, **d** AFT age

## Discussion

### Trend analysis of landslides occurrences over landscape attributes

The trend analysis of landslides occurrence across Teesta river catchment suggests that those regions which have influence of Indian Summer Monsoon (ISM) rainfall dominant during June–September months along the southern front has a higher frequency distribution of landslides occurrence than the region where rainfall intensity is low due to the topographic barrier, steeper slope gradient, higher relief change and minimum eroded rock column. The median trend for landslide occurrences for topographic variables is in between 1500–1700 m for elevation, 800–1000 m for relief, and 24°–28° for slope gradient, whereas for climatic variables, such as rainfall intensity, it ranges from 2500 to 2700 mm/year. In the Higher-Tethyan Himalaya regions, clusters of earthquake occurrences are associated by active seismicity, raising the possibility that these earthquakes could trigger large bedrock landslides to occur downstream. Most of the time, earthquakes have little impact on the amount of silt that is dumped into bedrock rivers downstream during high monsoon seasons. Earthquakes can be extrapolated to be a substantial factor for initiating bedrock landslides since they are a significant factor for bedrock landslides as a result of erosion in humid, medium-elevation settings (Bookhagen et al. 2005). It was also suggested that one of the most important hillslope erosion processes in the dry, high-elevation portions of the Himalayan terrain is erosion rate, which is significantly impacted by orographic lift during the monsoon season.

### Spatial relationship of tectonic and climate linkage in controlling landslides distribution over landscape evolution

Fluvial bedrock incision has a significant impact on limiting denudation rate process and controlling the relief formation of the landscape (Whipple and Tucker 1999; Godard et al. 2004; Safran et al. 2005). The hillslope growth process often acts as a passive regulator of the variation in fluvial incision rates. The adjoining hillslopes became steeper due to an increase in fluvial incision rates, which is countered by rapid bedrock landsliding. It appears that as fluvial incision rates decline, the relief structure in the downstream segment will also decrease, further lowering the rates of bedrock landsliding on the adjacent hillslopes. The Teesta River Catchment's limiting hillslopes are at the threshold slope angle for failure process, and the spatially uniform hillslope angles are created by the close geomorphic channel-gradient

coupling (Burbank et al. 1996; Harvey 2002). Despite significant gradients in uplift rates, rainfall intensity, erosional efficiency, and lithological settings, the slope distribution of the examined catchment is astonishingly consistent, with the exception of sub-catchment S1–S2. The presence of such optimal hillslopes indicates that drainage density, rather than fluvial incision rates or rock uplift, determines the local topographic relief (Burbank 2002). Therefore, considering complete geomorphic connection between stream networks and slope gradient, the fluvial incision would serve as the rate-limiting process, controlling the sediment transport in the non-glaciated landscape (Whipple and Tucker 1999).

Recent research suggests that the rates and patterns of denudation over the Himalayan region are controlled by tectonic-induced climate factors (Hodges et al. 2001, 2004; Burbank et al. 2003; Scherler et al. 2014). According to our analysis, there should be an inverse functional relationship between the variability of denudation rates and the exhumation rate in the Teesta catchment, as well as a linear functional relationship between rainfall intensity and denudation rates. Therefore, we conclude that the linear or inverse functional relationship between topographic variables, rainfall intensity, and exhumation rate can be linked to tectonic influence or lithological interference. It is also thought that a range of factors contribute to the variation in denudation rates and the link between denudation rates and topographic or climatic variables at the catchment scale, which is a significant parameter in understanding the dynamics of landslides in landscape evolution. In the given tectonically active and climatically varied catchment, the observed relationship between denudation rates, slope gradient, and topographic variables is linear, with denudation rates and exhumation rate is inversely proportional to increased topographic steepness. Given that bedrock landslides as a function of erosional proxy allow landscapes to become steep as a function of denudation rate, rising linear functional connections in the Himalayan catchment demonstrate this. The linear relationship between topographic steepness and topographic relief and geophysical relief may change due to a change in the relative strengths of topographic optimal slope failure rates (Burbank et al. 1996). The topography will be adequate to continue the steepness process to a greater level as denudation rates increase along the downstream segment, but it will also be susceptible to slope failure as the optimum slope angles are reached earlier as denudation rates rise. Our results indicate a linear proportional relationship between the channel steepness index and denudation rates, with landslides occurring more frequently as channel steepness rises in response to associated slope gradient and denudation rates. In order to provide surface runoff for catchment erosion efficiency, the findings also suggest that for regions with the lowest rainfall

rates, the mean denudation rates trend coincides linearly with the mean exhumation age trend. The highest denudation rates should be linked to high rainfall intensity, such as in the Indian summer monsoon period, if rainfall intensity affects the efficiency of erosion along a strike. Although it is thought that the mean annual rainfall may not be the primary determinant of how rainfall intensity affects the spatial variability of denudation rates. It has been proposed that erosion efficiency in bedrock terrain is modulated by the spatial variability of rainfall intensity over the seasonal distribution (Lague et al. 2005).

## Conclusion

The present study concluded that the spatial distribution of bedrock landslides occurrence over the controlling attributes such as topographic and rainfall variables show the highest probability of frequent landslides occurrence lies in the zones with  $\sim 24^{\circ}$ – $28^{\circ}$  of slope range,  $\sim 800$ – $1000$  m of relief range, in  $1500$ – $1700$  m elevation range, which coincides with the rainfall erosivity range of  $\sim 2500$ – $2700$  mm/year across the Teesta river catchment. We examined the relationship between the variability of erosion rates and topography variables, rainfall intensity, and exhumation rate over the Teesta river catchment to demonstrate the importance of topographic-climate coupling in moderating the variability of erosion rates. We observe an inverse functional relationship between the pattern of denudation rates and the variables determining the distribution of bedrock landslides, such as topographic matrices and rainfall intensity, and a direct proportional relationship between the two. Our analysis demonstrates the significance of spatial interrelationship of tectonic and climatic linkage in understanding the interaction between bedrock landslides induced landscape evolution in a tectonically active and highly dynamic orogen such as the eastern Himalaya. Further, in a highly active and dynamic orogen, the link between erosion rates and topographic variables is controlled by bedrock landslides and annual mean rainfall. As mean annual rainfall increases, the degree of linearity in the relation between denudation rate and topographic variables such slope gradient, topographic relief, geophysical relief, and Ksn increases. The results of our analysis demonstrate that topography and topographic steepness have a stronger linear relationship with changes in denudation rates in the lesser Himalayan sequence than in the higher to Tethyan Himalayan sequence. Our understanding of how these important earth surface processes interact globally will be greatly improved by future investigations on how these bedrock landslides' occurrence influences variations in erosion rates and topographic change in various tectonic setups. Understanding how landslides affect topography will help us better understand the interactions between

the variables influencing long-term landscape evolution and, ultimately, reducing landslide risk.

**Supplementary Information** The online version contains supplementary material available at <https://doi.org/10.1007/s12665-023-10859-6>.

**Acknowledgements** The Authors acknowledge the authorities of IIT Kharagpur for facilitating the study. AK thanks the Ministry of Education, Government of India for the grant of a Ph.D. Research Fellowship. Geological Survey of India (GSI-Bhukosh portal) for providing landslides inventory datasets.

**Author contributions** AK: conceptualization, methodology, formal analysis, data curation, validation, writing—original draft. MDB: conceptualization, supervision, writing—review and editing.

**Funding** The authors have not disclosed any funding.

**Availability of data and materials** On request, the corresponding author will provide the data that support the original study conclusions. Due to privacy or ethical constraints, the data are not publicly available.

## Declarations

**Conflict of interest** Authors declare that there is no potential conflict of interest.

## References

- Abbott LD, Silver EA, Anderson RS et al (1997) Measurement of tectonic surface uplift rate in a young collisional mountain belt. *Nature* 385:501–507
- Abrahami R, van der Beek P, Huyghe P et al (2016) Decoupling of long-term exhumation and short-term erosion rates in the Sikkim Himalaya. *Earth Planet Sci Lett* 433:76–88. <https://doi.org/10.1016/j.epsl.2015.10.039>
- Anbarasu K, Sengupta A, Gupta S, Sharma S (2010) Mechanism of activation of the Lanta Kholi landslide in Sikkim Himalayas. *Landslides* 7:135–147
- Andreani L, Stanek KP, Gloaguen R et al (2014) DEM-based analysis of interactions between tectonics and landscapes in the Ore Mountains and Eger Rift (East Germany and NW Czech Republic). *Remote Sens* 6:7971–8001
- Basu SR, De SK (2003) Causes and consequences of landslides in the Darjiling-Sikkim Himalayas, India. *Geogr Pol* 76:37–52
- Bhasin R, Grimstad E, Larsen JO et al (2002) Landslide hazards and mitigation measures at Gangtok, Sikkim Himalaya. *Eng Geol* 64:351–368
- Bhasin R, Shabanimashcool M, Hermanns R et al (2020) Back analysis of shear strength parameters of a large rock slide in Sikkim Himalaya. *J Rock Mech Tunn Technol* 26:81–92
- Bhattacharyya K, Mitra G (2009) A new kinematic evolutionary model for the growth of a duplex—an example from the Rangit duplex, Sikkim Himalaya, India. *Gondwana Res* 16:697–715
- BIS Code 1893 (2002) Earthquake hazard zoning map of India. Retrieved from [www.bis.org.in](http://www.bis.org.in)
- BMTPC (2003) Landslide hazard zonation atlas of India. Building Materials and Technology Promotion Council, Government of India and Anna University, Chennai, p. 125
- Bookhagen B, Burbank DW (2006) Topography, relief, and TRMM-derived rainfall variations along the Himalaya. *Geophys Res Lett* 33:L08405. <https://doi.org/10.1029/2006GL026037>

- Bookhagen B, Burbank DW (2010) Toward a complete Himalayan hydrological budget: spatiotemporal distribution of snowmelt and rainfall and their impact on river discharge. *J Geophys Res* 115:F03019. <https://doi.org/10.1029/2009JF001426>
- Bookhagen B, Thiede RC, Strecker MR (2005) Late Quaternary intensified monsoon phases control landscape evolution in the north-west Himalaya. *Geol* 33:149. <https://doi.org/10.1130/G20982.1>
- Brocklehurst SH, Whipple KX (2002) Glacial erosion and relief production in the Eastern Sierra Nevada, California. *Geomorphology* 42:1–24
- Brookfield M (1998) The evolution of the great river systems of southern Asia during the Cenozoic India-Asia collision: rivers draining southwards. *Geomorphology* 22:285–312
- Bull W (2007) *Tectonic Geomorphology of Mountains: A New Approach to Paleoseismology*, 320 pp. Blackwell, Oxford, UK, <https://doi.org/10.1002/9780470692318>
- Bull WB (2008) *Tectonic geomorphology of mountains: a new approach to paleoseismology*. Wiley, New York
- Burbank D (2002) Rates of erosion and their implications for exhumation. *Mineral Mag* 66:25–52
- Burbank DW, Leland J, Fielding E et al (1996) Bedrock incision, rock uplift and threshold hillslopes in the northwestern Himalayas. *Nature* 379:505–510
- Burbank D, Blythe A, Putkonen J et al (2003) Decoupling of erosion and rainfall in the Himalayas. *Nature* 426:652–655
- Burchfiel BC, Zhiliang C, Hodges KV, et al (1992) The South Tibetan Detachment System, Himalayan Orogen: Extension Contemporaneous with and Parallel to Shortening in a Collisional Mountain Belt. In: *Geological Society of America Special Papers*. Geological Society of America, pp 1–41. <https://doi.org/10.1130/SPE269-p1>
- Campforts B, Shobe CM, Overeem I, Tucker GE (2022) The art of landslides: how stochastic mass wasting shapes topography and influences landscape dynamics. *JGR Earth Surf*. <https://doi.org/10.1029/2022JF006745>
- Chakraborty T, Ghosh P (2010) The geomorphology and sedimentology of the Tista megafan, Darjeeling Himalaya: implications for megafan building processes. *Geomorphology* 115:252–266
- Flint J-J (1974) Stream gradient as a function of order, magnitude, and discharge. *Water Resour Res* 10:969–973
- Godard V, Cattin R, Lavé J (2004) Numerical modeling of mountain building: Interplay between erosion law and crustal rheology: INTERPLAY BETWEEN EROSION AND RHEOLOGY. *Geophys Res Lett*. <https://doi.org/10.1029/2004GL021006>
- Gupta V, Jamir I, Kumar V, Devi M (2017) Geomechanical characterisation of slopes for assessing rockfall hazards in the Upper Yamuna Valley, Northwest Higher Himalaya, India. *Himalayan Geol* 38:156–170
- Gupta V, Chauhan N, Penna I et al (2022) Geomorphic evaluation of landslides along the Teesta river valley, Sikkim Himalaya, India. *Geol J* 57:611–621. <https://doi.org/10.1002/gj.4377>
- Hack JT (1973) Stream-profile analysis and stream-gradient index. *J Res US Geol Surv* 1:421–429
- Harvey AM (2002) Effective timescales of coupling within fluvial systems. *Geomorphology* 44:175–201
- Hazarika P, Ravi Kumar M (2012) Seismicity and source parameters of moderate earthquakes in Sikkim Himalaya. *Nat Hazards* 62:937–952
- Hodges KV (2000) Tectonics of the Himalaya and southern Tibet from two perspectives. *Geol Soc Am Bull* 112:324–350
- Hodges KV, Hurtado JM, Whipple KX (2001) Southward extrusion of Tibetan crust and its effect on Himalayan tectonics. *Tectonics* 20:799–809. <https://doi.org/10.1029/2001TC001281>
- Hodges KV, Wobus C, Ruhl K et al (2004) Quaternary deformation, river steepening, and heavy rainfall at the front of the Higher Himalayan ranges. *Earth Planet Sci Lett* 220:379–389. [https://doi.org/10.1016/S0012-821X\(04\)00063-9](https://doi.org/10.1016/S0012-821X(04)00063-9)
- Jaiswara NK, Kotluri SK, Pandey AK, Pandey P (2019a) Transient basin as indicator of tectonic expressions in bedrock landscape: approach based on MATLAB geomorphic tool (Transient-profiler). *Geomorphology* 346:106853
- Jaiswara NK, Pandey P, Pandey AK (2019b) Mio-Pliocene piracy, relict landscape and drainage reorganization in the Namcha Barwa syntaxis zone of eastern Himalaya. *Sci Rep* 9:1–11
- Jaiswara NK, Kotluri SK, Pandey P, Pandey AK (2020) MATLAB functions for extracting hypsometry, stream-length gradient index, steepness index, chi gradient of channel and swath profiles from digital elevation model (DEM) and other spatial data for landscape characterisation. *Appl Comput Geosci* 7:100033
- Jamir I, Gupta V, Thong GT, Kumar V (2020) Litho-tectonic and rainfall implications on landslides, Yamuna valley, NW Himalaya. *Phys Geogr* 41:365–388. <https://doi.org/10.1080/0272346.2019.1672024>
- Keller EA, Pinter N (1996) *Active tectonics*. Prentice Hall, Upper Saddle River
- Keller EA, Pinter N (2002) *Active Tectonics: Earthquakes, Uplift, and Landscape*. Prentice Hall
- Kellett DA, Grujic D, Coutand I, et al (2013) The South Tibetan detachment system facilitates ultra rapid cooling of granulite-facies rocks in Sikkim Himalaya: S. TIBETAN DETACHMENT, SIKKIM HIMALAYA. *Tectonics* 32:252–270. <https://doi.org/10.1002/tect.20014>
- Kellett D, Grujic D, Mot-tram C, et al (2014) Virtual field guide for the Darjeeling-Sikkim Himalaya India. *Geological field trips in the Himalaya Karakoram and Tibet Journal of the Virtual Explorer, Electronic Edition*, ISSN 1441–8142. <https://doi.org/10.3809/jvirtex.2014.00344>
- Kirby E, Whipple KX (2012) Expression of active tectonics in erosional landscapes. *J Struct Geol* 44:54–75
- Kirby E, Snyder N, Spyropoloul K, Sheehan D (2005) Tectonics from topography: Procedures, promise and pitfalls. *Geomorphic and Thermochronologic Signatures of Active Tectonics in the Central Nepalese Himalaya* 17
- Koons PO (1989) The topographic evolution of collisional mountain belts; a numerical look at the Southern Alps, New Zealand. *Am J Sci* 289:1041–1069. <https://doi.org/10.2475/ajs.289.9.1041>
- Korup O, Clague JJ, Hermanns RL et al (2007) Giant landslides, topography, and erosion. *Earth Planet Sci Lett* 261:578–589. <https://doi.org/10.1016/j.epsl.2007.07.025>
- Korup O, Densmore AL, Schlunegger F (2010) The role of landslides in mountain range evolution. *Geomorphology* 120:77–90. <https://doi.org/10.1016/j.geomorph.2009.09.017>
- Krishna AP (2005) Snow and glacier cover assessment in the high mountains of Sikkim Himalaya. *Hydrol Process: Int J* 19:2375–2383
- Kumar V, Jamir I, Gupta V, Bhasin RK (2021) Inferring potential landslide damming using slope stability, geomorphic constraints, and run-out analysis: a case study from the NW Himalaya. *Earth Surf Dyn* 9:351–377. <https://doi.org/10.5194/esurf-9-351-2021>
- Lague D, Hovius N, Davy P (2005) Discharge, discharge variability, and the bedrock channel profile: DISCHARGE VARIABILITY AND CHANNEL PROFILE. *J Geophys Res*. <https://doi.org/10.1029/2004JF000259>
- Lehner B, Verdin K, Jarvis A (2008) New global hydrography derived from spaceborne elevation data. *Eos Trans AGU* 89:93. <https://doi.org/10.1029/2008EO100001>
- Liu G, Einsele G (1994) Sedimentary history of the Tethyan basin in the Tibetan Himalayas. *Geol Rundsch* 83:32–61
- Mehrotra G, Sarkar S, Kanungo D, Mahadevaiah K (1996) Terrain analysis and spatial assessment of landslide hazards in parts of Sikkim Himalaya. *J Geol Soc India* 47:491–498

- Mitra G, Bhattacharyya K, Mukul M (2010) The lesser Himalayan duplex in Sikkim: implications for variations in Himalayan shortening. *J Geol Soc India* 75:289–301
- Montgomery DR, Brandon MT (2002) Topographic controls on erosion rates in tectonically active mountain ranges. *Earth Planet Sci Lett* 201:481–489
- Montgomery DR, Balco G, Willett SD (2001) Climate, tectonics, and the morphology of the Andes. *Geology* 29:579. [https://doi.org/10.1130/0091-7613\(2001\)029%3c0579:CTATMO%3e2.0.CO;2](https://doi.org/10.1130/0091-7613(2001)029%3c0579:CTATMO%3e2.0.CO;2)
- Mukul M (2000) The geometry and kinematics of the Main Boundary Thrust and related neotectonics in the Darjiling Himalayan fold-and-thrust belt, West Bengal, India. *J Struct Geol* 22:1261–1283
- Mukul M (2010) First-order kinematics of wedge-scale active Himalayan deformation: insights from Darjiling–Sikkim–Tibet (DaSiT) wedge. *J Asian Earth Sci* 39:645–657
- O’Callaghan JF, Mark DM (1984) The extraction of drainage networks from digital elevation data. *Comput vis Graph Image Process* 28:323–344
- Safran EB, Bierman PR, Aalto R et al (2005) Erosion rates driven by channel network incision in the Bolivian Andes. *Earth Surf Process Landf J Br Geomorphol Res Group* 30:1007–1024
- Scherler D, Bookhagen B, Strecker MR (2014) Tectonic control on <sup>10</sup>Be-derived erosion rates in the Garhwal Himalaya, India. *J Geophys Res Earth Surf* 119:83–105
- Schumm SA (1979) Geomorphic Thresholds: The Concept and Its Applications. *Trans Inst Brit Geograph* 4:485. <https://doi.org/10.2307/622211>
- Schwanghart W, Scherler D (2014) TopoToolbox 2–MATLAB-based software for topographic analysis and modeling in Earth surface sciences. *Earth Surf Dyn* 2:1–7
- Singh KK, Singh A (2016) Detection of 2011 Sikkim earthquake-induced landslides using neuro-fuzzy classifier and digital elevation model. *Nat Hazards* 83:1027–1044
- Small EE, Anderson RS (1998) Pleistocene relief production in Laramide mountain ranges, western United States. *Geology* 26:123–126
- Strahler AN (1952) Hypsometric (area-altitude) analysis of erosional topography. *Geol Soc Am Bull* 63:1117–1142
- Weidinger JT, Korup O (2009) Frictionite as evidence for a large Late Quaternary rockslide near Kanchenjunga, Sikkim Himalayas, India—implications for extreme events in mountain relief destruction. *Geomorphology* 103:57–65
- Whipple KX, Tucker GE (1999) Dynamics of the stream-power river incision model: implications for height limits of mountain ranges, landscape response timescales, and research needs. *J Geophys Res: Solid Earth* 104:17661–17674
- Whipple KX, DiBiase RA, Crosby BT (2013) 9.28 Bedrock Rivers. In: *Treatise on Geomorphology*. Elsevier, pp 550–573
- Whittaker AC, Cowie PA, Attal M et al (2007) Bedrock channel adjustment to tectonic forcing: implications for predicting river incision rates. *Geology* 35:103. <https://doi.org/10.1130/G23106A.1>
- Wobus C, Whipple KX, Kirby E, et al (2006) Tectonics from topography: Procedures, promise, and pitfalls. In: *Tectonics, Climate, and Landscape Evolution*. Geological Society of America
- Yin A (2006) Cenozoic tectonic evolution of the Himalayan orogen as constrained by along-strike variation of structural geometry, exhumation history, and foreland sedimentation. *Earth Sci Rev* 76:1–131. <https://doi.org/10.1016/j.earscirev.2005.05.004>

**Publisher's Note** Springer Nature remains neutral with regard to jurisdictional claims in published maps and institutional affiliations.

Springer Nature or its licensor (e.g. a society or other partner) holds exclusive rights to this article under a publishing agreement with the author(s) or other rightsholder(s); author self-archiving of the accepted manuscript version of this article is solely governed by the terms of such publishing agreement and applicable law.